Electrochimica Acta 307 (2019) 253–259

Contents lists available at ScienceDirect

Electrochimica Acta

journal homepage: www.elsevier.com/locate/electacta

Electrocatalysis driven high energy density Li-ion polysulfide battery

Abdulrazzag Sawas, Ganguli Babu, Naresh Kumar Thangavel, Leela Mohana Reddy Arava*

Department of Mechanical Engineering, Wayne State University, 5050 Anthony Wayne Drive, Detroit, MI, 48202-3902, United States

ARTICLE INFO

Article history:
Received 22 October 2018
Received in revised form
26 February 2019
Accepted 27 March 2019
Available online 29 March 2019

Keywords:
Electrocatalysis of polysulfides
Porous silicon anodes
Li-ion polysulfide battery
Li-S battery
Polarization

ABSTRACT

Though carbon-based porous materials have improved lithium-sulfur (Li-S) battery performance remarkably, the poor adsorption of polysulfides and their sluggish reaction kinetics limits them from practical application. On the other hand, the presence of lithium metal especially under the highly reactive polysulfide environment causes safety concerns. Herein, we use electrocatalytically active cathode and metallic lithium-free anode to construct Li-ion polysulfide battery with enhanced reversibility and safety. Stabilizing lithium polysulfides and enhancing the reaction kinetics with minimal polarization using platinum/graphene composite holds the key to obtaining better performance, which is realized against conventional metallic lithium as well as pre-lithiated porous silicon electrodes. The electrocatalyst containing cathode composites are comparable with graphene-based electrodes regarding enhanced specific capacity retention and better reversibility in charge/discharge behavior. Furthermore, metallic lithium-free polysulfide batteries displayed exceptional performance with an energy density of 450 Wh kg^{-1} considering the weight of both the electroactive materials and a capacity retention of about 70% for 240 charge-discharge cycles.

1. Introduction

Li-ion batteries are today's ultimate energy storage system boosting the mobile world, power-hungry laptops, and other portable electronics. These rechargeable power sources have been at the forefront of energy storage systems due to the unique combination of high energy density and light weight [1]. However, if the future energy needs are taken into account, the current pace of technological progress will be unable to sustain the demand due to their limited energy storage electrodes (graphite and $LiMnO_2$) [2]. Beyond the limitations of Li-ion batteries (typically around 150–200 Wh kg^{-1}), lithium-sulfur (Li-S) system is promising owing to its low cost and high theoretical energy density (~2567 Wh kg^{-1}), safety, a wide temperature range of operation and eco-friendliness of the sulfur electrode [2–5]. Nevertheless, practical applications of the Li-S battery are hindered by issues like short cycle life, poor coulombic efficiency, poisoning of Li anode, self-discharge, etc. [4,6–8]. Such performance limitations are generally originated from the insulating nature of sulfur and parasitic reactions of its discharge products with the highly reactive negative electrode (metallic lithium) [6].

Remarkable achievements have been accomplished on the sulfur electrode side (cathode) through confinement approaches using a wide variety of carbon materials, conducting polymers, metal oxides and electrocatalytically active electrodes [9–16]. Though it causes equal problems as that of the sulfur cathode, research spotlight on lithium anode is not as much as its counterpart. Moreover, the presence of lithium metal is unsafe for any rechargeable Li-battery due to dendrite formation, mossy metal deposits and its possibility to penetrate through a separator (causing an internal short circuit) during the charge/discharge process [17,18]. Despite recent advances in the protection of the metallic lithium electrode, success is limited due to lack of stability of the passivation layer, especially upon continuous cycling in Li–S batteries [19–22].

To realize the practical applications with high energy density and safety, constructing a metallic lithium-free negative electrode for a rechargeable sulfur-based battery is not only an immediate necessity but also a challenging task. In this regard, silicon (Si) is a favorable alternative electrode for metallic-lithium due to its high theoretical capacity and lower alloying/de-alloying potential vs. Li/Li^+ [22,23]. However, to combat its large volume expansion during the charge-discharge process, nanotechnology-based methodologies have been used as contemporary research efforts to stabilize their structural integrity [23,24]. Among various architectures, three dimensional (3-D) porous silicon electrodes are capable of

* Corresponding author.
E-mail address: leela.arava@wayne.edu (L.M.R. Arava).

https://doi.org/10.1016/j.electacta.2019.03.191
0013-4686/

reducing internal stresses/fracture upon electrode expansion and compression during the charge-discharge cycling process [24–26]. To make use of the best of high capacity electrodes such as sulfur and silicon, it is a prerequisite that lithium should be incorporated into either cathode or anode prior to cell assembly.

For integration of Li, Aurbach et al. reported the full cell configuration based on lithiated silicon and sulfur-carbon composite with a specific capacity of 600 mAh/g for initial cycles [27,28]. However, drastic capacity fade is observed after ten cycles with an increase in the internal resistance due to the formation of a thicker passivation layer possibly on either of the electrodes upon cycling. Consequently, other pioneer researchers also demonstrated the feasibility of the system using various lithiated silicon structures or Li_2S as starting materials [28–31]. For instance, Li-S full cell concept is demonstrated using lithium sulfide against aluminum and graphite anodes [32]. Similarly, a Li-ion sulfur battery was fabricated using carbon coated lithium sulfide (Li_2S) and electrodeposited silicon [30]. Most of these reports use carbons as a conductive matrix for cathodes, which is believed not to be effective to trap dissolved lithium polysulfides (LiPS) due to their non-polar nature [33–35]. In the same line, though the sulfur composites with carbons replete with a wide range of workable potential window, an increase in internal resistance over cycling makes them unsuitable for practical applications [23,27,28,30]. Recently, we have shown that the polar-natured metals on graphene have a strong affinity towards negatively charged dissolved polysulfides [36–38] which traps and eventually converts them electrocatalytically on the cathode surface [39]. Such a process provides stability against polarization and eventually leads to long cycle life in a narrow working potential window. Hence, based on their catalytic properties towards LiPS conversion reactions, selective electrocatalysts on graphene nanosheets could enhance reaction kinetics by decreasing internal resistance in the full cell configuration. Herein, we successfully revealed that the combination of electrocatalytically active composite cathode with 3-D porous metallic lithium-free anode are optimum to build high energy density and safer Li-ion polysulfide systems.

2. Experimental section

2.1. Preparation of electrocatalyst-anchored-graphene composite cathode

Electrocatalyst-anchored-graphene (Gr) composite is prepared using a polyol approach, wherein functionalized graphene (200 mg) was added into ethylene glycol (200 mL) with an effective stirring under Argon gas flow. Then, calculated amount of hexachloroplatinic acid (H_2PtCl_6) was added as platinum (Pt) source with a continuous stirring and heating at 180 °C. After refluxing the solution for about 8 h with sodium borohydride ($NaBH_4$) at pH 11, the suspended Pt anchored graphene composite was collected and filtered, which was then dried at 90 °C for 12 h. Typical step-by-step procedure for graphene functionalization and polyol reduction process has been reported elsewhere [37].

2.2. Fabrication of electrode material

3-D porous silicon electrodes were fabricated using electrodeposited porous nickel (Ni) on stainless steel as current collectors. Amorphous silicon was deposited conformally by plasma enhanced chemical vapor deposition (PECVD) on pre-deposited porous Ni/stainless steel substrate. The uniform conformal Si coating was achieved by tuning experimental parameters such as carrier/reacting gas (N_2/SiH_4) mixture flow, substrate temperature, chamber pressure, and deposition time. Details pertinent to the preparation of three-dimensional porous Ni current collectors which in turn morph into silicon electrodes are reported previously [26,40]. The mass loading of Si coated on Ni was found to be 0.5 mg/cm^2 per electrode and this value was used for capacity normalization. Electrochemical lithiation of 3-D Si was performed by fabricating cells with 3-D Si as working electrode, metallic lithium as a counter/reference electrode and 1 M of lithium bis (trifluoromethanesulfonyl) imide (LiTFSI) in triethylene glycol dimethyl ether (TEGDME) as an electrolyte with celgard as a separator.

2.3. Coin cell fabrication

Standard 2032-coin cells were used to construct half cells and full cell sulfur battery configurations. Graphene composite is mixed with conductive carbon (Super-P) and polyvinylidene fluoride (PVDF) binder in the weight ratio of 80: 10: 10 using N-methyl-2-pyrrolidone (NMP) solvent to obtain a thick slurry. Such slurry was applied on an aluminum foil current collector and dried in an oven at 80 °C to evaporate NMP solvent. Prior to use as a cathode, the coated electrode was roll pressed to get uniform thickness. The Gr and lithiated porous silicon were used as-such to construct their respective half cells and full cell configurations. Half cells were assembled using above-said electrodes as working electrodes and lithium metal as counter cum reference electrode. To prepare full cells, known molar concentration (0.6 M Li_2S_8) of catholyte was used as the active material as a part of electrolyte which consists of 1 M LiTFSI and lithium nitrate (0.5 M, $LiNO_3$) in TEGDME solvent and Celgard as a separator. Li-ion polysulfide full cells were fabricated by matching the capacities of individual electrodes in respective half-cell configurations.

2.4. Characterizations

The morphology of the electrodes before and after cycling was characterized by a JSM 401F (JEOL Ltd., Tokyo, Japan) SEM and a JEM 2010 (JEOL Ltd, Tokyo, Japan) SEM. Cyclic voltammograms (CV) and electrochemical impedance spectra's (EIS) were recorded in the potential range from 1.5 to 0.05 V and the frequency range from 100 kHz to 100 MHz respectively using Bio-logic (SP-200) electrochemical workstation. Charge-discharge studies at different current rates (from C/10 to 1 C rate) were carried out on ARBIN charge-discharge cycle life tester.

3. Results and discussion

To eliminate the explosive and expensive metallic lithium anode and to retain the performance of sulfur cathode, a high capacity 3-D porous silicon electrode was used to assemble high energy density Li-ion polysulfide battery. Silicon electrodes were assembled with desired porosity using engineered Ni current collectors as reported in our earlier studies [26,40]. Firstly, porous Ni current collectors were prepared by selective etch-out of Copper (Cu) component from electrodeposited Cu-Ni alloy. Then 3-D silicon electrodes were attained by the conformal coating of amorphous Si on porous Ni using PECVD method. Fig. 1a shows the scanning electron microscopy (SEM) images corresponding to the cross-sectional view of porous Ni current collector deposited on stainless-steel substrate and inset shows the top view. Uniform pore size (~1 μm), pore distribution and thickness (~5 μm) were achieved by optimizing the electrodeposition procedure. Conformal coating of Si on such current collectors was performed with an optimized thickness of 0.5 μm, as confirmed from a thickness profiler and SEM images (Fig. 1b).

Fig. 1c represents the cyclic voltammograms of 3-D Si electrode

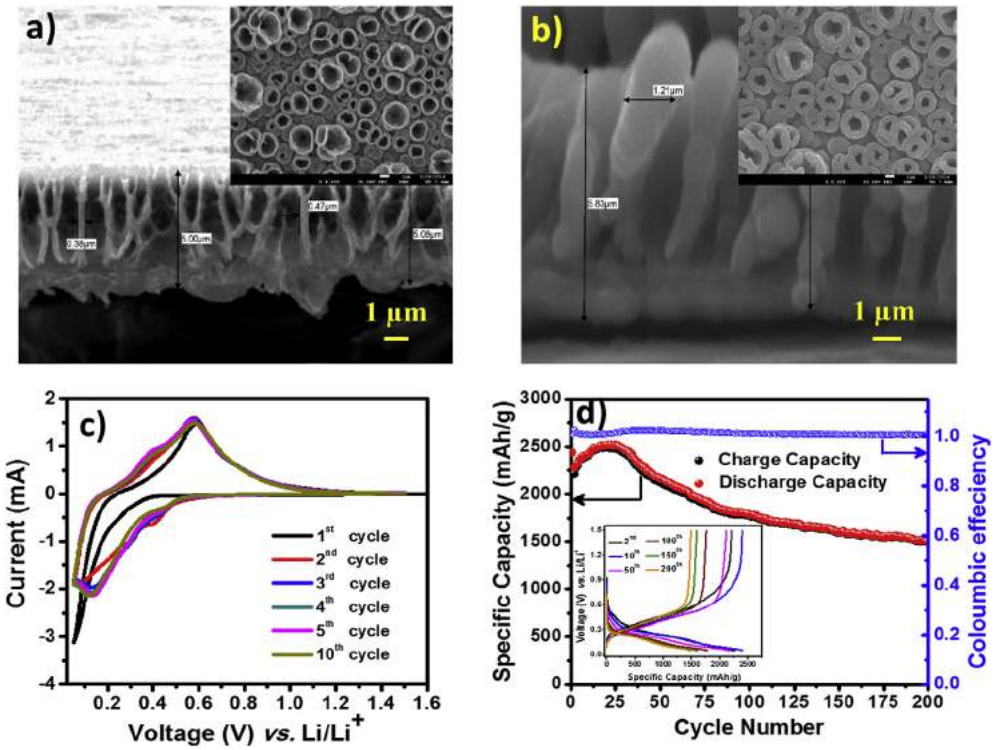

Fig. 1. Cross sectional SEM images of a) porous Ni current collector (inset-top view), b) PECVD coated Si to form 3-D porous electrode, c) cyclic voltammograms of 3-D Si *vs.* Li/Li^+ in the potential range of 0.05–1.5 V at a scan rate of 0.1 mV/s and d) cycling performance of 3-D Si electrode at a current rate of 0.2C. (For interpretation of the references to colour in this figure legend, the reader is referred to the Web version of this article.)

in the potential range of 1.5–0.05 V vs. Li/Li^+ at a scan rate of 0.1 mV s^{-1}. A distinctive difference between the first and second cycle is due to the formation of solid-electrolyte interphase (SEI), generally associated with the film-like growth during initial lithiation of Si electrode. The large current in a first backward scan from 0.34 to 0.05 V is attributed to Li-rich Li-Si phase, the reduction in peak currents and broadening of the peak (0.49–0.05 V) on subsequent CV scans reveal the formation and charging (double layer capacitance) of the passivation film. On the forward scan, current peaks at 0.19, 0.38 and 0.58 V were observed due to the de-lithiation from the Li-Si phases. Thus, the perfect overlapping of redox peaks with repeated cycling confirms the stability and integrity of silicon electrodes. Further, galvanostatic charge-discharge studies of 3-D Si electrode at a constant current rate of 0.2C were performed, and the obtained results are displayed in Fig. 1d. From the inset of Fig. 1d, it was observed that Si electrode displayed well-defined discharge-charge plateaus corresponding to the lithiation and de-lithiation process. Herein, the consistency in voltage profiles upon cycling is characteristics of amorphous silicon coated conformally on 3-D Ni current collectors. Remarkably, the capacities for first discharge and charge were 2430 and 2210 mAh g^{-1} respectively, signifying a coulombic efficiency of 91% with minimal loss of capacity during SEI formation. A slight increase in specific capacity appeared for early cycles owing to the improved utilization of silicon electrode as test progressed. From the cycling characteristics, a stable coulombic efficiency was observed (99.5%) with minimal capacity fade with progressive cycling. However, capacity retention behavior was improved for further cycling, for instance, 16% capacity loss for second hundred cycles against 39% for first hundred cycles demonstrates the stability of 3-D Si for long cycling full cell applications. Additionally, the performance at high currents such as C/2 and C-rates was also exceptional with specific capacities of 2210 and 1830 mAh g^{-1} respectively (Fig. S1), and corroborates the high rate capability of silicon electrodes.

On the other hand, cathode half-cell was constructed with an electrocatalyst-containing Graphene composite and was evaluated in comparison with pristine graphene in regard to LiPS conversion reactions. Fig. 2a shows a SEM image of as-prepared graphene which reveals randomly oriented nanosheets with several microns in lateral size and ripple-like paper morphology. However, Pt functionalized graphene sheets (Fig. 2b) shows the spatial presence of Pt nanoparticles with a uniform size of 5 nm which is attributed to an efficient glycol-reduction process. To assess the electrocatalytic activity of Pt/Graphene and Graphene against polysulfides, three-electrode cyclic voltammetry (CV) experiments were performed at 0.05 mV/s scan rate and shown in Fig. 2c. During cathodic sweep, anodic shift in reduction potential and large current density were observed at intermediate LiPS reaction for Pt/Graphene (2.25 V vs. Li/Li^+) compared to the Graphene electrodes (2.22 V vs. Li/Li^+) indicating facile conversion of LiPS from soluble to insoluble state (Li_2S/Li_2S_2) on Pt surface. The accelerated reaction kinetics on Pt is ascribed to its polar nature and electronic conductivity which helps in adsorption of liquid LiPS (Lewis acid-base interaction) and to convert them into the end products in an effective manner. Such an interaction reduces the polysulfide shuttling effect in the cell and increases the discharge capacity. Similarly, in reverse sweep, a more cathodic shift in LiPS oxidation potential and enhanced current density were obtained on Pt/Graphene (2.42 V vs. Li/Li^+) compared to the Graphene electrode (2.47 V vs. Li/Li^+). More importantly, the peak at 2.2 V corresponds to the decomposition of Li_2S, that is essential for sequential oxidation process for solid sulfur formation, is much pronounced in Pt/Graphene which indicates the enhanced kinetics of LiPS oxidation reaction. Thus, the electrocatalytic surface certainly influences the reversibility of reaction which is always beneficial to obtain improved cycle life performance along with round-trip efficiency.

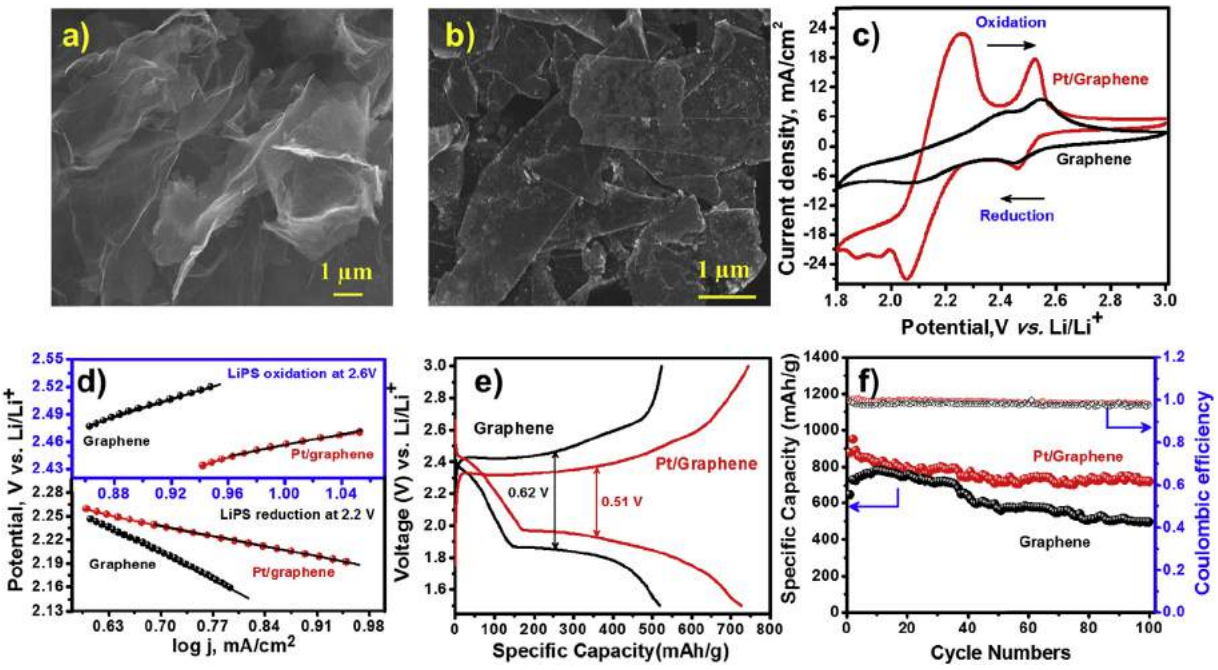

Fig. 2. FE-SEM images of a) pristine graphene,b) Pt nanoparticles decorated graphene sheets, c) three-electrode cyclic voltammogram of LiPS redox reaction on pristine graphene (black) and Pt/graphene (red). Scan rate: 0.05 mV/s d) Tafel analysis (η vs. log j mA/cm^2) on LiPS redox reaction, e) galvanostatic charge-discharge profiles and f) cycling performance. (For interpretation of the references to colour in this figure legend, the reader is referred to the Web version of this article.)

To elucidate the catalytic surface effect on LiPS redox, kinetic analysis such as Tafel slope measurements were performed from the linear region of polarization curve, as shown in Fig. 2d. The Pt/Graphene shows Tafel slope value of 178 mV/dec and 274 mV/dec for reduction and oxidation processes respectively, which were very low compared to that of Graphene. In addition, exchange current densities obtained from extrapolation of the current axis in Tafel plot were found to be higher on Pt/Graphene ($1.5*10^{-2}$ A/cm^2 for reduction and $8.03*10^{-3}$A/cm^2 for oxidation) surface compared to the Graphene ($6.51*10^{-3}$ A/cm^2 for reduction and $5.63*10^{-3}$A/cm^2 for oxidation). The obtained low Tafel slope and higher exchange current density values of Pt/Graphene surface corroborates its electrocatalytic activity on LiPS redox reactions. Hence, having electrocatalytic materials as a cathode host surface apparently reduces the Li-S cell polarization and enhances the cycle life performance by lowering the redox overpotentials and accelerating the LiPS reaction kinetics. To appraise electrochemical cycling behavior, charge-discharge measurements were performed at 0.2C rate in the potential range between 1.5 and 3.0 V. In order to have a fair comparison, the concentration and amount of LiPS (600 mM and 10 µl) and electrolyte were kept constant during cell fabrication.

Fig. 2e depicts the comparative charge/discharge plateaus of pristine Graphene and Pt/Graphene electrodes in a view to monitor polarization differences upon long cycling. Both the electrodes exhibit two distinctive discharge plateaus at 2.4 and 2.0 V corresponding to formation of medium-chain LiPS (Li_2S_n $n \geq 4$) and short-chain LiPS (Li_2S_n $n = 1–3$) respectively. Herein, Pt/Graphene electrode exhibits reduced polarization, at any depth of discharge, with a value of 0.51 V compared to 0.62 V for pristine Graphene which indicates the facile reaction kinetics enhancement for LiPS conversion reactions in case of Pt/Graphene. More notably, charging at lower potential suggests the conversion of short-chain to long-chain polysulfides, which are more electrochemically active and helps to limit the loss of active mass in the form insoluble Li_2S, thereby enhancing the cycle life. The retention of specific capacity of the electrodes over the number cycles has been displayed in Fig. 2f. The Pt/Graphene electrode exhibits a specific capacity of 810 mAh/g at a current rate of 0.2C while the graphene electrode shows about 620 mAh/g with a gradual capacity fade over 100 cycles. Though initial capacities are comparable for both the electrodes, a clear difference was seen in capacity retention over the cycling due to the incapability of adsorbing and converting short-chain LiPS on the pristine graphene electrodes. Such stability of the capacity values on Pt/Graphene electrode is attributed to its inherent properties such as high conductivity of composite, polysulfide absorption, and conversion ability. At the end of the 100th cycle, Pt/Graphene electrode exhibited a capacity of 732 mAh g^{-1} with a capacity retention of about 86%, whereas pristine Graphene electrode delivered as low as 471 mAh g^{-1} (~50%) representing improved LiPS reversibility. Hence, electrocatalytically active metals like Pt are crucial to enhance LiPS reversibility and reaction kinetics by protecting active surface for further reactions, and thus Pt/Graphene can serve as host for LiPS on the cathode side for Li-ion polysulfide full cell configurations.

For the fabrication of full cell Li-ion polysulfide batteries, prelithiated 3-D porous silicon was taken as an anode and Pt/Graphene as a cathode in a TEGDME electrolyte containing 0.6 M polysulfides. For better comparison, pristine graphene cathode was also used to build a full cell in an identical manner to realize the effect of electrocatalysis on electrochemical performance. To balance the full cell configurations, the weight of silicon and sulfur in the form of polysulfides have been matched with respect to their individual specific capacities on half-cells. As prelithiated Si was used in the anode, the fabricated cell was in a charged state with an open circuit voltage of about 2.1 V. Thus the test started with discharging to 1.5 V at a current rate of 0.2C. Fig. 3a displays charge-discharge plateaus of Li-ion polysulfide battery with pristine Graphene cathode wherein profiles are signature of sulfur electrode with average discharge voltage around 1.82 V. Though it exhibits high initial capacity of 600 mAh g^{-1} owing to the nanosheets layers accommodating the polysulfides, a rapid capacity loss within a few cycles was seen which indicates the poor adsorption capability of

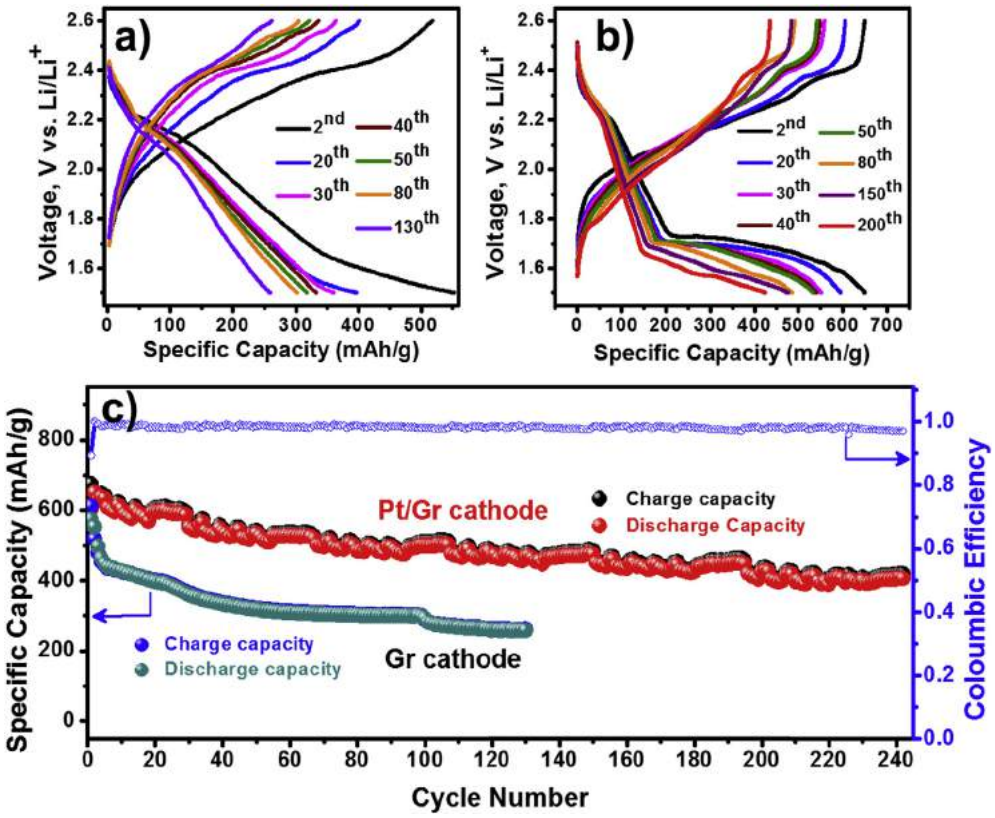

Fig. 3. Charge/discharge profiles of Li-ion polysulfide battery a) Graphene, b) electrocatalytically active Pt/graphene composite as positive electrodes vs. Li_xSi as negative electrode and c) cycling performance of Li-ion polysulfide batteries at 0.5C.

sulphiphobic Graphene surface followed by gradual capacity fade with cycling. Notably, steady increase in the polarization with cycling is possibly due to the solution resistance originating from the ineffective conversion of LiPS and inherently poor conductivity of both electrodes (Graphene and Si). Furthermore, deposition of insulative species of short-chain LiPS on the electrode's surface worsen the situation, thus the second discharge plateau disappears from the voltage range investigated (Fig. 3a and 40th cycle). Hence, it is clear that usage of high capacity electrodes such as silicon and sulfur to construct high energy density storage system is entirely reliant on regulated polarization via. utilization of LiPS and its effective reversibility. The underlying mechanism would be reduction in activation energy for polysulfide conversion reactions by catalytically active cathode surface and thus enabling battery operation in a narrow potential window.

Interestingly, catalyst-containing Pt/Graphene cathode based full cell showed minimal change in discharge plateaus with an increased number of cycles, which is an indication of the enhanced reversibility of polysulfides during charge/discharge process. Herein, Pt plays a constructive role in improving reaction kinetics and thereby protecting surface active sites for further redox reactions, as understood from the voltage profiles (Fig. 3b). Furthermore, we have observed the stable specific capacity for Li-ion polysulfide cell that consists of Pt/Graphene cathode over 240 cycles with 0.147% of capacity loss per cycle, while Graphene electrodes has 2.6% capacity loss per cycle for the first 10 cycles followed by 0.54% capacity loss per cycle over 130 cycles, could endure only about 100 cycles. Due to the inherent electrochemical activity of Pt particles, they largely have control over polarization in the charge-discharge process (Fig. 3c) and delivers stable capacity of about 597 mAh g^{-1} with extended cycle life. It is noteworthy to know that the Pt/Graphene cell exhibits almost double the energy density of commercial Li-ion batteries (450 Wh kg^{-1}, based on the weight of both electrode materials) with 70% capacity retention even after 240 charge-discharge cycles. Such exceptional performance of currently studied Li-ion polysulfide cells is attributed to the combination of catalytically active Pt/Graphene cathodes and 3-D porous silicon anodes as evidenced from the excellent capacity retention and coulombic efficiency. Contrarily, the catalyst-free electrode is not feasible to build metallic lithium-free high energy density batteries even though it provides high capacity at initial cycles.

In order to understand the reversibility of lithium polysulfides conversion reactions and their impedance behavior, cyclic voltammetry (CV) and electrochemical impedance spectroscopic (EIS) studies have been performed on Li-ion polysulfides full cell configuration. Fig. 4a shows that representative CVs at a scan rate of 0.2 mV s^{-1} which consist of two reduction peaks at 2.2 and 1.7 V, corresponding to conversion of elemental sulfur to higher order polysulfide (Li_2S_8) and lower order lithium polysulfides (Li_2S_2 and Li_2S) respectively. Upon the forward scan, a broad oxidation peak at about 2.1 V and a sharp peak at 2.4 V were seen owing to reversible conversion of lower order LiPS to higher order ones and sulfur respectively. Herein, oxidation peaks, especially the broad peak at 2.1 V is quite different from that of the sulfur half-cell (vs. Li/Li^+, Fig. S2) possibly due to poor conductivity and slightly higher lithiation potential in the full cell configuration. To get further insights, we have fabricated three-electrode configuration cells with a platinum wire as a third reference electrode, provided all other parameters remain unaltered (Fig. S3). Based on the results, it was concluded that the counter electrode plays a crucial role in altering not only the shape of the CV but also shifting the potentials of redox

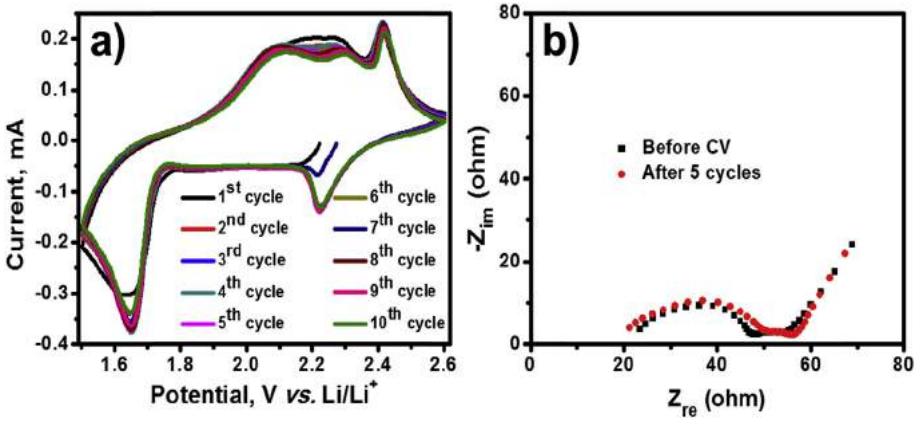

Fig. 4. a) Cyclic voltammograms b) Electrochemical impedance Nyquist spectra of Li-ion polysulfide battery consisting of electrocatalytically active Pt/Graphene electrode.

reactions marginally. However, overlapping of curves as the number of CV scans increases strongly suggest the robustness of the system and capability of long cycling.

Further, electrochemical impedance behavior of individual electrodes and the full cell with their combination was investigated to understand the internal resistance changes that influence the overpotential and polarization. As expected, solution resistance was about 20 Ω which is slightly higher compared to the polysulfides-free electrolyte (Fig. 4b and Fig. S4). It is important to note that solution resistance remains constant as cycling proceeded, due to the excellent reversible nature of polysulfides by electrocatalytically active electrode. This process indicates the absence of unreacted dissolved polysulfides in the electrolyte. Similarly, minimal change in interfacial resistance was observed with cycling due to the facile kinetics of conversion reactions originated by Pt-containing an electrode. Hence, the present full cell configuration is feasible for long cycling within the operable potential window. On the other hand, the impedance was measured in equilibrium conditions before cycling and after five charge-discharge cycles, in both the configurations such as individual electrodes vs. Li/Li^+ and their full cell configuration. Typical Nyquist plots of 3-D porous silicon and Pt/Graphene are shown in Fig. S4a and b, respectively. At high-frequency region, the spectra indicates the ionic conductivity of polysulfide free electrolyte to be about 12.5 Ω, which is used to fabricate silicon half cells. As the frequency sweeps to lower values, the spectra appear as a depressed semicircle with the diameter representing the charge-transfer resistance (10.5 Ω) which mostly depends on the passivation layer present on the silicon electrode. On the other hand, the polysulfides containing electrolyte with Pt/graphene electrode vs. Li/Li^+ exhibits a slightly higher resistance of 19 Ω possibly due to the presence of insulating nature of sulfur species. Similarly, the charge-transfer resistance of the Li-S half-cell exhibits marginally higher value of about 54Ω as contributed by more number of resistive elements in the electrode.

4. Conclusion

In summary, electrocatalyst-containing cathode composite was used to catalyze lithium polysulfide reversibly with reduced overpotential especially with prolonged cycling. Silicon morphs into a 3-D porous structure and was pre-lithiated to be uses as a metallic lithium-free anode against lithium polysulfides on Pt-graphene composite cathode. Such a novel configuration of the Li-ion polysulfide battery revealed a specific capacity of 597 mAh g^{-1} with 70% capacity retention over 240 cycles. The exceptional electrochemical performance was attributed to the improved reaction kinetics by the inherent electrochemical activity of Pt/Graphene electrode and structural stability of 3D Si anodes. Finally, the full cell exhibited an energy density of 450 Wh kg^{-1} with an average voltage of 1.9 V, which is almost double that of the commercial Li-ion batteries.

Acknowledgement

This article was supported in part by the NSF Division of Chemical, Bioengineering, Environmental, and Transport Systems (CBET: 1748363).

Appendix A. Supplementary data

Supplementary data to this article can be found online at https://doi.org/10.1016/j.electacta.2019.03.191.

References

[1] D. Aurbach, Y. Gofer, Z. Lu, A. Schechter, O. Chusid, H. Gizbar, Y. Cohen, V. Ashkenazi, M. Moshkovich, R. Turgeman, J. Power Sources 97 (2001) 28–32.
[2] M.M. Thackeray, C. Wolverton, E.D. Isaacs, Energy. Environ. Sci. 5 (2012) 7854–7863.
[3] J. Cabana, L. Monconduit, D. Larcher, M.R. Palacin, Adv. Mater. 22 (2010) E170–E192.
[4] P.G. Bruce, S.A. Freunberger, L.J. Hardwick, J.-M. Tarascon, Nat. Mater. 11 (2012) 19–29.
[5] A. Fotouhi, D.J. Auger, K. Propp, S. Longo, M. Wild, Renew. Sustain. Energy Rev. 56 (2016) 1008–1021.
[6] D. Lv, J. Zheng, Q. Li, X. Xie, S. Ferrara, Z. Nie, L.B. Mehdi, N.D. Browning, J.G. Zhang, G.L. Graff, Adv. Energy. Mater. 5 (2015) 1400290–1400298.
[7] A. Manthiram, Y. Fu, S.H. Chung, C. Zu, Y.S. Su, Chem. Rev. 114 (2014) 11751–11787.
[8] D. Bresser, S. Passerini, B. Scrosati, Chem. Commun. 49 (2013) 10545–10562.
[9] D.W. Wang, Q. Zeng, G. Zhou, L. Yin, F. Li, H.M. Cheng, I.R. Gentle, G.Q.M. Lu, J. Mater. Chem. A. 1 (2013) 9382–9394.
[10] Q. Pang, X. Liang, C.Y. Kwok, L.F. Nazar, Nat. Energy. 1 (2016) 16132–16138.
[11] X. Fan, W. Sun, F. Meng, A. Xing, J. Liu, Green. Energy. Environ. 3 (2018) 2–19.
[12] D. Liu, C. Zhang, G. Zhou, W. Lv, G. Ling, L. Zhi, Q.H. Yang, Adv. Sci. 5 (2018) 1700270–1700282.
[13] X. Liu, J.Q. Huang, Q. Zhang, L. Mai, Adv. Mater. 29 (2017) 1601759–1601765.
[14] H.J. Peng, G. Zhang, X. Chen, Z.W. Zhang, W.T. Xu, J.Q. Huang, Q. Zhang, Angew. Chem. Int. Ed. 55 (2016) 12990–12995.
[15] H.B. Lin, L.Q. Yang, X. Jiang, G.C. Li, T.R. Zhang, Q.F. Yao, G.W. Zheng, J.Y. Lee, Energy. Environ. Sci. 10 (2017) 1476–1486.
[16] Y. Yang, G. Yu, J.J. Cha, H. Wu, M. Vosgueritchian, Y. Yao, Z. Bao, Y. Cui, ACS Nano 5 (2011) 9187–9193.
[17] X.B. Cheng, R. Zhang, C.Z. Zhao, Q. Zhang, Chem. Rev. 117 (2017) 10403–10473.
[18] W. Xu, J. Wang, F. Ding, X. Chen, E. Nasybulin, Y. Zhang, J.-G. Zhang, Energy. Environ. Sci. 7 (2014) 513–537.
[19] S.S. Zhang, Electrochim. Acta 70 (2012) 344–348.
[20] B.D. Adams, E.V. Carino, J.G. Connell, K.S. Han, R. Cao, J. Chen, J. Zheng, Q. Li, K.T. Mueller, W.A. Henderson, J.-G. Zhang, Nano Energy 40 (2017) 607–617.
[21] Y. Lu, S. Gu, X. Hong, K. Rui, X. Huang, J. Jin, C. Chen, J. Yang, Z. Wen, Energy.

Storage. Mater 11 (2018) 16–23.
[22] T. Tao, S. Lu, Y. Fan, W. Lei, S. Huang, Y. Chen, Adv. Mater. 29 (2017) 1700542–1700561.
[23] M. Piwko, T. Kuntze, S. Winkler, S. Straach, P. Härtel, H. Althues, S. Kaskel, J. Power Sources 351 (2017) 183–191.
[24] Z. Zhang, Y. Wang, W. Ren, Q. Tan, Y. Chen, H. Li, Z. Zhong, F. Su, Angew. Chem. Int. Ed. 126 (2014) 5265–5269.
[25] L. Lin, X. Xu, C. Chu, M.K. Majeed, J. Yang, Angew. Chem. Int. Ed. 55 (2016) 14063–14066.
[26] K. Ababtain, G. Babu, X. Lin, M.-T.F. Rodrigues, H. Gullapalli, P.M. Ajayan, M.W. Grinstaff, L.M.R. Arava, ACS App. Mater. Interface. 8 (2016) 15242–15249.
[27] R. Elazari, G. Salitra, G. Gershinsky, A. Garsuch, A. Panchenko, D. Aurbach, Electrochem. Commun. 14 (2012) 21–24.
[28] M. Hagen, E. Quiroga-González, S. Dörfler, G. Fahrer, J. Tübke, M.J. Hoffmann, H. Althues, R. Speck, M. Krampfert, S. Kaskel, H. Föll, J. Power Sources 248 (2014) 1058–1066.
[29] H. Jha, I. Buchberger, X. Cui, S. Meini, H.A. Gasteiger, J. Electrochem. Soc. 162 (2015) A1829–A1835.
[30] M. Agostini, J. Hassoun, J. Liu, M. Jeong, H. Nara, T. Momma, T. Osaka, Y.K. Sun, B. Scrosati, ACS App. Mater. Interface. 6 (2014) 10924–10928.
[31] Y. Yan, Y.-X. Yin, S. Xin, J. Su, Y.G. Guo, L.J. Wan, Electrochim. Acta 91 (2013) 58–61.
[32] L. Wang, Y. Wang, Y. Xia, Energy. Environ. Sci. 8 (2015) 1551–1558.
[33] J. Liang, Z.H. Sun, F. Li, H.M. Cheng, Energy. Storage. Mater. 2 (2016) 76–106.
[34] X. Ji, K.T. Lee, L.F. Nazar, Nat. Mater. 8 (2009) 500–506.
[35] B. Ding, C. Yuan, L. Shen, G. Xu, P. Nie, X. Zhang, Chem. Eur J. 19 (2013) 1013–1019.
[36] G. Babu, K. Ababtain, K.Y.S. Ng, L.M.R. Arava, Sci. Rep. 5 (2015) 8763.
[37] H. Al Salem, G. Babu, C.V. Rao, L.M.R. Arava, J. Am. Chem. Soc. 137 (2015) 11542–11545.
[38] G. Babu, N. Masurkar, H. Al Salem, L.M.R. Arava, J. Am. Chem. Soc. 139 (2017) 171–178.
[39] N.K. Thangavel, D. Gopalakrishnan, L.M.R. Arava, J. Phys. Chem. C 121 (2017) 12718–12725.
[40] S.R. Gowda, V. Pushparaj, S. Herle, G. Girishkumar, J.G. Gordon, H. Gullapalli, X. Zhan, P.M. Ajayan, A.L.M. Reddy, Nano Lett. 12 (2012) 6060–6065.